

Quadruped Molecular Anchoring to an Insulator: Functionalized Ferrocene on CaF₂ Bulk and Thin Film Surfaces

Linda Laflör, Fabian A. Schlage, Lev Kantorovich, Philip J. Moriarty, Michael Reichling, and Philipp Rahe*

Cite This: *J. Phys. Chem. C* 2020, 124, 9900–9907

Read Online

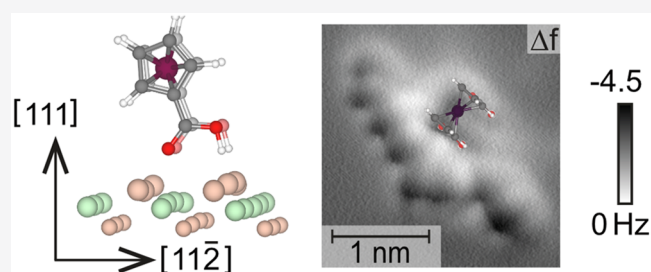
ACCESS |

Metrics & More

Article Recommendations

Supporting Information

ABSTRACT: The formation of insulator-supported functional molecular structures requires a firm anchoring of the molecular building blocks to the underlying surface. With a suitable anchoring mechanism, the functionality of single molecules can be maintained and molecular reaction routes for advanced fabrication can be realized to ultimately produce a functional unit. Here, we demonstrate the anchoring of a functionalized ferrocene molecule 1,1'-ferrocenedicarboxylic acid (FDCA) to the CaF₂(111) surface. Due to the large band gap and high purity of CaF₂ crystals, as well as the presence of particularly large, defect-free terraces, CaF₂(111) is a prototypical insulator surface most suitable for the fabrication of molecular devices. Noncontact atomic force (NC-AFM) and scanning tunneling microscopy (STM) experiments performed on CaF₂ bulk and CaF₂/CaF₁/Si(111) thin film samples reveal the formation of ultrasmall molecular FDCA islands composed of only a few molecules. This molecular assembly is stable even at room temperature and at temperatures as low as 5 K. A comparison of the experimental data with results of density functional theory (DFT) calculations indicates that the exceptional stability is based on a robust quadruped binding motif. This quadruped anchoring bears strong potential for creating tailored molecular structures on CaF₂(111) surfaces that are stable at room temperature.



INTRODUCTION

Motivated by applications in the fields of catalysis, molecular electronic devices, or molecular (opto-)electronics, there is now a large body of work available where the principles and strategies of molecular structure formation on surfaces have been studied.^{1,2} Molecular self-assembly and on-surface synthesis routes have been identified as promising approaches to form complex functional structures, especially on metal surfaces.^{1,3} However, applications addressing the molecular conductivity or molecular charge state usually require insulating supports.^{4–7}

On-surface molecular assembly is subject to a quintessential competition between two key interactions, namely, molecule–molecule and molecule–substrate bonds. On metallic surfaces, these two interactions can often be well separated via tuning of the molecule–molecule interaction by attachment of specific functional groups while the molecule–substrate interaction can often be tailored independently by controlling the electronic hybridization or dispersion forces between the metallic surface and a molecular backbone.^{1,2} On insulator surfaces, in contrast, electronic hybridization is absent and dispersion forces are often not sufficient to hinder dewetting at room temperature.⁸ Instead, molecular anchoring, where specific end groups bind the molecule to specific surface sites, has been identified as a

route to structure formation and enabled the realization of advanced reaction routes on insulating supports.^{9–11}

A key parameter for assessing molecular anchoring is the molecule–surface bond strength.⁹ Thus, molecular assembly enabled by anchoring usually relies on surface-induced templating, where the molecular superstructure follows the geometry of the underlying surface lattice.¹² Successful examples of molecular anchoring, where molecules have been observed to form templated structures on insulator surfaces stable at room temperature, include molecules with cyano groups binding to step edges on KBr(001),¹³ molecules with flexible cyano groups binding to KCl(001),¹⁴ or molecules with carboxylic acid groups binding to calcite(104).^{9,15} On CaF₂(111) surfaces, a cooperative anchoring mechanism to stabilize small molecular assemblies of cytosine has been identified,¹⁶ while the molecule–surface bond between 3,4,9,10-perylenetetracarboxylic diimide (PTCDI), as well as

Received: January 6, 2020

Revised: February 21, 2020

Published: February 27, 2020



chloro(subphthalocyaninato)boron(III) (SubPc) molecules, and $\text{CaF}_2(111)$ has been found to be rather weak.^{17,18}

Functionalized ferrocene molecules are promising building blocks for functional structures as they link tailored anchor groups with an active center; plain ferrocene is, for example, widely used as a reference redox system in electrochemistry.¹⁹ Ferrocene molecules functionalized by two carboxylic acid moieties, namely, 1,1'-ferrocenedicarboxylic acid (FDCA), have been investigated on calcite(104)⁶ as well as on $\text{Ag}(111)$, $\text{Au}(111)$, $\text{Cu}(110)$, and $\text{Cu}_3\text{N}/\text{Cu}(110)$ surfaces²⁰ before. Deprotonation of the carboxylic acid groups has been observed on $\text{Cu}(110)$ and $\text{Cu}_3\text{N}/\text{Cu}(110)$ surfaces, leading to upright-standing molecules as a consequence of a strong molecule–surface interaction.²⁰ For other systems, deprotonation does not occur and, instead, intact molecules are observed to arrange into a (2×1) superstructure on calcite(104),⁶ while they form complex self-assembled patterns on Ag and Au surfaces.²⁰

In this study, we identify a quadruped molecular anchoring motif from the interaction of FDCA with $\text{CaF}_2(111)$ surfaces of bulk crystals and thin films grown on $\text{Si}(111)$. The anchoring allows for the formation of room-temperature stable assemblies as well as the observation of single isolated molecules at 300 K and is a case study for a system exhibiting strong molecule–surface and weak molecule–molecule interactions. Results from noncontact atomic force (NC-AFM) and scanning tunneling microscopy (STM) experiments are complemented by ab initio calculations using density functional theory (DFT). The combination of these experimental and theoretical approaches unravels the molecular adsorption characteristics, including details regarding the molecule–surface bond formation.

METHODS

Sample preparation and scanning probe microscopy experiments were performed under ultrahigh vacuum conditions ($p < 5 \times 10^{-10}$ mbar) in four separate vacuum systems. An overview of the systems is given in Table 1.

Table 1. Experimental Conditions Used within This Study (T: Measurement Temperature)

system	type	mode	sample	T (K)
A	Omicron LT gen.II	NC-AFM, STM	thin film	5, 77
B	Omicron LT gen.III	NC-AFM	bulk	5
C	Omicron VT STM 25	STM	thin film	300
D	RHK Beetle VT AFM	NC-AFM	bulk	300

Sample Preparation. Thin film CaF_2 surfaces were prepared in two steps. First, flash cycles yield the (7×7) reconstruction on highly B-doped p-type $\text{Si}(111)$ samples (Institute of Electronic Materials Technology, Warsaw, Poland). Next, CaF_2 material (cleanliness 99.9%, Alfa Aesar, Kandel, Germany) was deposited from an EFM3T e-beam evaporator (Focus GmbH, Huenstetten, Germany) on the $\text{Si}(111)$ surface held at about 600 °C. The CaF_1 interface layer forms at this temperature and enables CaF_2 multilayer growth; further details can be found in ref 21. Bulk CaF_2 samples (Korth Kristalle, Altenholz, Germany) were prepared by cleaving in vacuum after degassing the crystal and sample holder.²² The sample was heated at about 330 K for 1 h before molecule deposition and NC-AFM experiments on system B, while it was directly used without heating on system D.

The $[11\bar{2}]$ surface direction is determined experimentally as follows: CaF_2 bulk crystals are cleaved along another $\{111\}$ plane after the experiments, and the $[11\bar{2}]$ direction points toward the obtuse edge of the produced $\{111\}$ surface. On the thin film samples, the CaF_2 $[11\bar{2}]$ direction can be determined by inspecting the orientation of the (7×7) unit cell of silicon in STM as CaF_2 films are grown in type-B epitaxy.²¹

Molecule Evaporation. Homebuilt Knudsen cells were filled with 1,1'-ferrocenedicarboxylic acid material (cleanliness 98%, Alfa Aesar, Kandel, Germany). The compound was degassed for several days for further purification before deposition. FDCA was evaporated at about 390 K on samples held at room temperature.

Scanning Probe Microscopy. Low-temperature STM and NC-AFM measurements on thin film samples were performed at 5 and 77 K with an Omicron LT qPlus gen.II instrument (ScientaOmicron GmbH, Taunusstein, Germany) using a MATRIX control system (system A). Tuning-fork sensors in qPlus configuration²³ with a W-tip and a separate tip wire were used in this system. Despite the presence of electrostatic background forces, NC-AFM experiments on thin film samples were performed at sample bias of $U_s=0$ V to exclude cross-talk between the NC-AFM and tunneling current signals.²⁴ Low-temperature NC-AFM experiments on bulk CaF_2 samples were performed with an Omicron LT qPlus gen.III instrument connected to a MATRIX control system (system B). qPlus sensors as supplied by the manufacturer were used in this system. Room-temperature STM data on CaF_2 thin film samples were acquired with an Omicron VT AFM 25 controlled by a MATRIX system and using W-tips (system C). Room-temperature NC-AFM measurements on bulk samples were performed using an RHK beetle-type AFM UHV 750 instrument (RHK Technology, Troy MI, USA) operated by an RHK R9 control system (system D). Ar-sputtered Si cantilevers (type PPP-NCH from Nanosensors, Neuchâtel, Switzerland) with eigenfrequencies of around $f_0 \sim 300$ kHz were used in an optical beam-deflection configuration. For charge compensation, a sample bias of typically -5 V was applied to minimize the electrostatic background forces. All experimental data were analyzed using Gwyddion.²⁵

Density Functional Theory Calculations. Calculations were performed with the CP2K (www.cp2k.org) code.²⁶ Mixed Gaussian and plane waves were used together with the MOLOPT short-range basis sets of double- ζ quality^{27,28} and Goedecker–Teter–Hutter (GTH) potentials²⁹ using the Perdew–Burke–Ernzerhof (PBE) generalized gradient approximation (GGA) functional³⁰ and the Γ point sampling. Van der Waals interactions were included using the Grimme DFT-D3 dispersion correction,³¹ as implemented in CP2K. Results were cross-checked using the nonlocal rVV10 method,³² yielding systematically higher adsorption energies but similar molecular geometries. The basis-set superposition error is included in the adsorption energies and was calculated using the counterpoise (CP) method.³³ The adsorption energies were all calculated with respect to the staggered FDCA gas-phase geometry.

For the geometry optimization of single FDCA molecules, the $\text{CaF}_2(111)$ surface was modeled by a 5×5 , 6-layer CaF_2 slab with the lowest CaF_2 layer fixed in the bulk geometry. Three CaF_2 triple layers (lowest triple layer fixed) and a 6×6 surface unit cell were used for calculating dimer geometries. The 1×10^{-4} Ha/Bohr force tolerance has been used in geometry optimization calculations.

The electron density difference is calculated as $\Delta\rho = \rho_{\text{slab+FDCA}} - \rho_{\text{slab}} - \rho_{\text{FDCA}}$, whereby $\rho_{\text{slab+FDCA}}$ is the electron density of the full system, while ρ_{slab} and ρ_{FDCA} denote the electron densities of the $\text{CaF}_2(111)$ slab and the FDCA molecule, respectively. CP-corrected dimer binding energies $E_{\text{dimer}}^{\text{CP}}$ are calculated as $E_{\text{dimer}}^{\text{CP}} = E_{\text{dimer,total}}^{\text{CP}} - E_{\text{slab}} - 2E_{\text{FDCA}}$ with the 2-body CP-corrected total dimer energy $E_{\text{dimer,total}}^{\text{CP}}$ and the energies of the separately geometry-optimized slab (E_{slab}) and FDCA (E_{FDCA}) subsystems. The energy gain/loss is calculated by comparison with two FDCA/ $\text{CaF}_2(111)$ monomers: $E_{\text{diff}} = E_{\text{dimer}}^{\text{CP}} - 2E_{\text{monomer}}^{\text{CP}}$.

RESULTS AND DISCUSSION

NC-AFM and STM experiments were performed in situ after depositing FDCA to a coverage between about 0.02 and 0.2 FDCA/nm² on bulk and thin film CaF_2 samples. The samples were held at room temperature during deposition; see *Methods* for further details.

$\text{CaF}_2(111)$ surfaces are terminated by a layer of fluoride ions with F–Ca–F triple layers stacked along the (111) direction; see *Figure 1a*. Bulk $\text{CaF}_2(111)$ surfaces were prepared by in situ cleaving, leading to surfaces with large, defect-free terraces.^{34,35} For the growth of CaF_2 thin films on Si(111) we chose preparation parameters, where CaF_2 multilayers grow on top of a CaF_1 interface layer, the latter being the result of an interface reaction between CaF_2 molecules and the Si(111)-(7 × 7) surface.^{21,36,37} Because of only a small lattice mismatch (0.6% at 300 K) between CaF_2 and the underlying silicon, the atomic structures of the bulk and thin film (111) surfaces are virtually identical. Thus, the main difference between the $\text{CaF}_2(111)$ bulk and thin film surface is the presence of the underlying CaF_1 interface layer binding to the silicon surface for the thin film sample; see *Figure 1b*, where the structure of a single CaF_2 layer on $\text{CaF}_1/\text{Si}(111)$ is shown. Samples are usually prepared in a way that both $\text{CaF}_2/\text{CaF}_1/\text{Si}(111)$ and $\text{CaF}_1/\text{Si}(111)$ areas are present at the surface.

While the CaF_2 layer is virtually defect-free, atomic-size defects within the CaF_1 interface layer have been identified by high-resolution NC-AFM imaging.²¹ Therefore, we herein do not investigate the properties of FDCA molecules on the CaF_1 interface layer.

Figure 1c,d presents NC-AFM and STM data acquired on $\text{CaF}_2(111)$ bulk and thin film samples, respectively, where small clusters of molecules are revealed; exemplary clusters are marked by arrows. In NC-AFM imaging, the smallest unit observed within these clusters is a pair of dark depressions embedded in a bright halo, which we will herein refer to as dumbbells. Exemplary dumbbells are marked in *Figure 1c* by white ellipses. Due to the large band gap of CaF_2 , STM experiments can only be performed on the thin film samples. In the respective STM data, the smallest unit observed is an elliptical protrusion; two examples are marked in *Figure 1d*. The dumbbell and elliptical shapes will, in the following, be identified as single FDCA molecules.

From a total of 347 and 243 clusters measured on bulk and thin film surfaces, respectively, at coverages ranging from 0.02 to 0.2 FDCA/nm², we extract the occurrence of the number of cluster-forming units having the dumbbell or elliptical shape with the results shown in *Figure 1e* (data for bulk and thin film samples are shown in red and yellow, respectively). Under all conditions, namely, bulk and thin film samples investigated with NC-AFM and STM at 300 K, 77 K, or 5 K (see the Supporting Information *Figure S1* for a full data overview), we

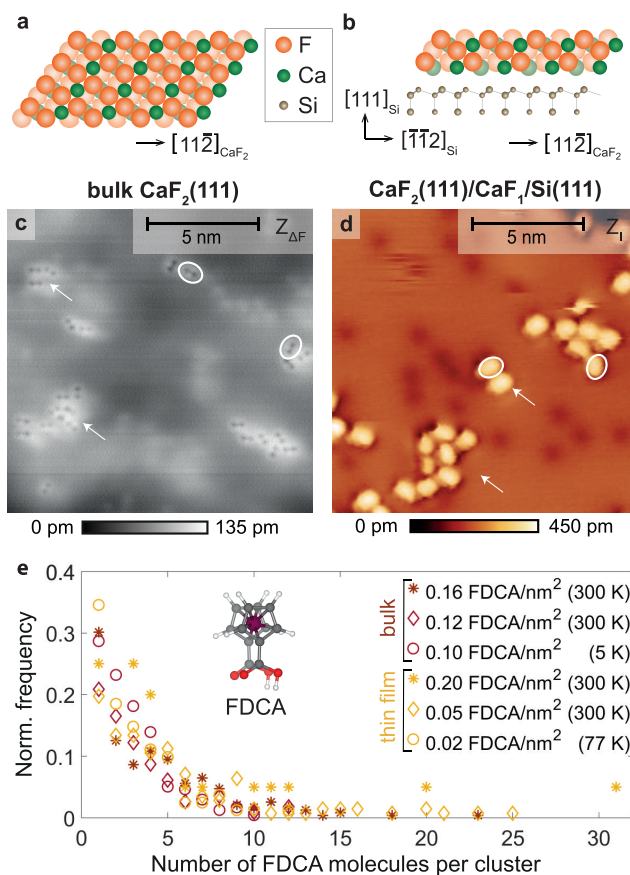


Figure 1. FDCA molecules deposited on the bulk and thin film $\text{CaF}_2(111)$ surfaces. (a, b) Cross-sectional models of the bulk and thin film surface systems. (c) NC-AFM measurement on a bulk sample at 5 K and (d) STM measurement on a thin film sample at 300 K. Single FDCA molecules and small FDCA clusters are marked by ellipses and arrows, respectively. (e) Normalized FDCA cluster size distribution for different $\text{CaF}_2(111)$ surfaces. Results for bulk crystal (thin film) samples are plotted in red (yellow). The respective coverage and measurement temperature are given in the legend. Molecular deposition was performed with the samples held at room temperature. Imaging conditions: (c) NC-AFM with a qPlus sensor ($f_0 = 26641$ Hz) at $\Delta f = -5.5$ Hz, $U_S = 4$ V, $T = 5$ K; (d) STM at $I = 2$ pA, $U_S = -3$ V, $T = 300$ K.

observe very small and stable FDCA assemblies, including the presence of single FDCA molecules. Specifically, the island size density distribution in *Figure 1e* reveals no significant difference in the functional dependence of the normalized abundance of the island sizes for the different samples; for both surfaces, more than 85% of the islands contain 10 or less molecules. The observation of similar distributions for the bulk and thin film surfaces suggests a negligible influence of the underlying CaF_1 interface layer on the assembly. As bulk $\text{CaF}_2(111)$ surfaces are known to exhibit an exceedingly low defect density,^{34,35} the similarity of the distribution functions for bulk and thin film surfaces furthermore suggests a similarly low defect density for the thin film CaF_2 layer. In contrast, mostly single FDCA molecules are found on the CaF_1 interface layer (data not shown), where a large number of defects have indeed been observed.²¹

Finding similar adsorption properties for FDCA on $\text{CaF}_2(111)$ bulk and thin film samples is markedly different from studies performed for 3,4,9,10-perylenetetracarboxylic dianhydride (PTCDA) on NaCl(001) and KBr(001) bulk and

thin film surfaces.^{38–40} In the latter examples, distinct differences in the on-bulk and on-thin film molecular structures have been observed.

Detailed NC-AFM and STM images of the same molecular cluster containing five of the aforementioned units are shown in Figure 2a,b. There is a good match between the scaled ball-

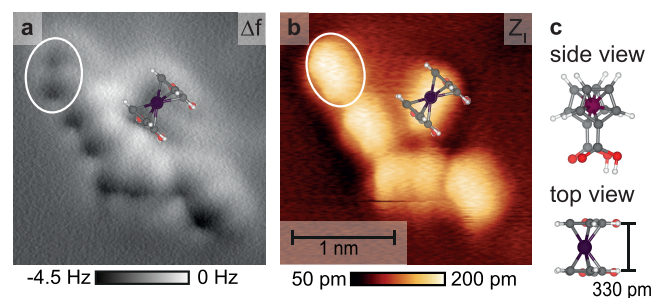


Figure 2. Imaging one FDCA cluster with NC-AFM and STM. (a, b) FDCA cluster formed by five molecules imaged in constant-height NC-AFM and constant-current STM. (a) Molecules appear as dumbbells in NC-AFM constant-height frequency-shift data. (b) Elliptical protrusions are apparent in STM data. A to-scale model of a single FDCA molecule is overlaid in the experimental data. Additionally, a single FDCA molecule, which was manipulated while scanning, is marked by a white ellipse. (c) Model of FDCA in eclipsed conformation. Imaging conditions: (a) constant-height NC-AFM image acquired with a qPlus sensor ($f_0 = 26641$ Hz) at $U_S = 0$ V, $T = 77$ K. A 4 pixel averaging filter was applied to the image data; (b) STM at $I = 2$ pA, $U_S = -3$ V, $T = 77$ K.

and-stick FDCA model (overlaid on the experimental data in Figure 2a,b) and one dumbbell imaged in NC-AFM, as well as one elliptical protrusion imaged in STM. In particular, we measure from the images an average distance between the two dumbbell depressions in the NC-AFM data of 500 ± 100 pm, which is close to the separation of 330 pm between the two cyclopentadienyl (Cp) rings of a single FDCA molecule in the FDCA bulk structure (see Figure 2c), but does not match the distance of about 900 pm between the Fe centers of the two nearest FDCA molecules in the bulk dimer structure.^{41,42} Thus, we identify one protrusion in STM as one single FDCA molecule, while the NC-AFM appearance of a single molecule is the dumbbell shape with two depressions surrounded by a bright halo. This interpretation is supported by the observation that a single feature can be manipulated by the scanning tip as happened with the molecule marked in Figure 2a,b within an image (not shown) acquired between the NC-AFM and STM data presented in Figure 2.

To clarify the adsorption geometry and molecular orientation, we performed density functional theory (DFT)-based geometry optimization calculations (using the CP2K package²⁶) for a single FDCA molecule adsorbed on a $\text{CaF}_2(111)$ slab in a total of eight FDCA/ $\text{CaF}_2(111)$ starting geometries. (See Methods and the Supporting Information for more details.) The most stable adsorption geometry (geo 1) found across all investigated structures is shown in Figure 3. The FDCA molecule takes an “eclipsed” conformation, where the two carboxylic acid groups point to the same direction. As a consequence, both Cp rings and carboxylic acid groups are located on top of each other. Although this eclipsed conformation is also adapted in the bulk structure,⁴² we found for an isolated gas-phase FDCA molecule a preference for a partly “staggered” conformation, where the rings are

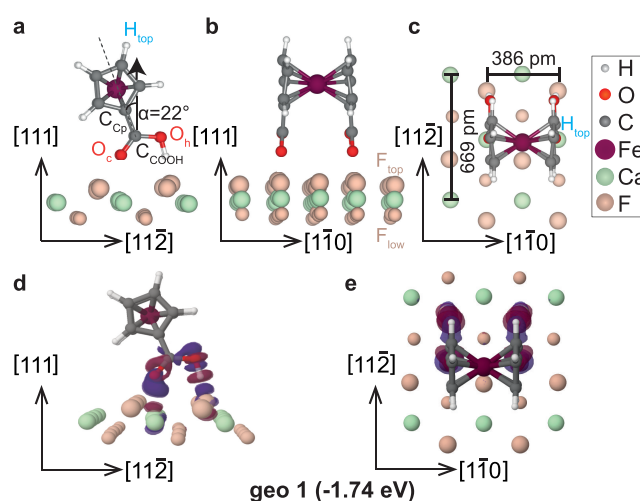


Figure 3. Adsorption geometry geo 1 of FDCA on $\text{CaF}_2(111)$. (a, b) Side and (c) top views of FDCA/ $\text{CaF}_2(111)$ in the DFT-optimized geometry (for clarity, only the top CaF_2 layer is shown). (d) Side and (e) top views of the electron density difference $\Delta\rho$ with isosurfaces at -0.015 $\text{e}/\text{\AA}^3$ (red) and 0.015 $\text{e}/\text{\AA}^3$ (blue).

rotated by about 60° toward each other, with an energy gain of about -0.06 eV (see the Supporting Information, Figure S2).

In the minimum energy geometry geo 1, the carboxylic acid groups point toward the $\text{CaF}_2(111)$ surface and are in plane with the linked Cp rings. The carbonyl oxygens (O_c) are located on top of surface calcium ions, while the hydroxyl oxygen atoms (O_h) form bonds via the hydrogen atoms to top fluorine (F_{top}) surface atoms. The $\text{F}_{\text{top}}\text{--H--O}_h$ distance of 2.52 Å is in good agreement with the distance expected for a moderate-to-strong hydrogen bond,⁴³ and the Ca--O_c distance of 2.40 Å points toward a more pronounced interaction. The geometry is furthermore favored by the approximate match between the $\text{O}_h\text{--O}_c$ distance of 227 pm and the $\text{Ca--F}_{\text{top}}$ distance of 281 pm, and the side and top views in Figure 3b,c reveal a close match between the FDCA bulk structure Cp ring distance of 330 pm with the $\text{CaF}_2(111)$ surface unit cell size along $[1\bar{1}0]$ of 386 pm. An analysis of the electron density difference $\Delta\rho$ using isosurfaces of ± 0.015 $\text{e}/\text{\AA}^3$ (e being the elementary positive charge) is shown in Figure 3d,e. The bonding electron density is strongly localized at the carboxylic acid moieties and their nearby surface atoms, specifically along the two $\text{F}_{\text{top}}\text{--H--O}_h$ and the two Ca--O_c bonds. The result of the molecule–surface interaction is a slightly tilted molecular geometry with an angle α of the $\text{C}_{\text{COOH}}\text{--C}_{\text{Cp}}$ bond to the (111) surface normal of about 22° , as marked in Figure 3a. Consequently, the ferrocene subunit protrudes from the surface, with the highest point above the surface plane occupied by the two top hydrogen atoms H_{top} , one from each Cp ring. The resulting quadruped binding motif, where one may imagine the molecule standing on four feet on the surface, explains the experimental finding of room-temperature stable molecular adsorption as effectively a total of four entities bind rather independently, each in a favorable vertical geometry, to the $\text{CaF}_2(111)$ surface.

Next, by analyzing the molecular orientations and nearest-neighbor geometries, we provide evidence that the molecular assembly is templated by the $\text{CaF}_2(111)$ surface. The $\text{CaF}_2(111)$ surface belongs to the planar space group $p3m1$, while the planar space group of only the topmost fluoride layer would be $p6mm$. As the DFT-calculated, energetically preferred

FDCA geometry geo 1 includes interactions with F_{top} and Ca atoms, three equivalent adsorption positions on the surface following the 3-fold rotational $\text{CaF}_2(111)$ surface symmetry are expected. These equivalent orientations, which also include equivalent orientations due to the surface mirror symmetry, can be characterized by the alignment of the molecular Cp–Fe–Cp axis at 30° , 150° , and 270° with respect to the $[11\bar{2}]$ direction; see Figure 4a. However, as mirror-symmetric

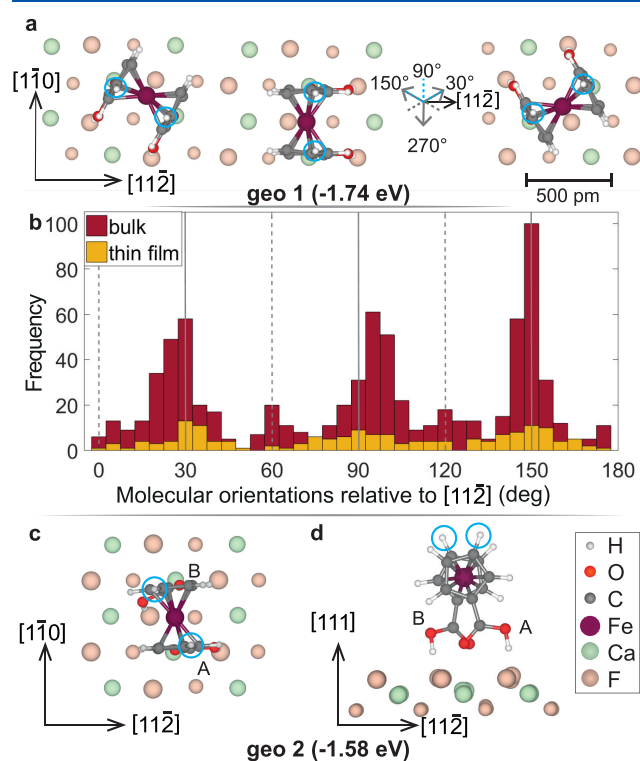


Figure 4. Analysis of molecular orientations. (a) Sketches of FDCA molecular orientations (geo 1) following the 3-fold rotational symmetry of the $\text{CaF}_2(111)$ surface. (b) Frequency of experimentally measured orientations for bulk (thin film) samples plotted in red (yellow), clearly showing the expected orientations of 30° , 90° , and 150° . Orientations are analyzed with respect to the $[11\bar{2}]$ surface direction. (c) Top and (d) side views of the DFT-optimized less favorable (metastable) molecular geometry (geo 2), explaining the intermediate peaks at about 0° , 60° , and 120° .

dumbbells (NC-AFM) or ellipses (STM) are typically observed in the experiments, the molecular orientations are only determined within the range of 0 – 180° , with the 270° orientation appearing at 90° . Thus, we expect to observe angles of 30° , 90° , and 150° for the Cp–Fe–Cp molecular axis from the experimental data. Due to the eclipsed Cp rings, the top hydrogen atoms (marked by blue circles in Figure 4a) producing the dumbbell contrast are aligned with the Cp–Fe–Cp axis.

The orientations of a total of 962 FDCA molecules were determined using the orientations of the dumbbell (NC-AFM) and elliptical (STM) shapes and with respect to the $[11\bar{2}]$ surface direction on bulk (788) and thin film (174) CaF_2 surfaces, yielding the angular distribution histograms shown in Figure 4b. On thin film samples, molecules bound to step edges were ignored. No step edges were observed within the images on CaF_2 bulk samples. Across the range of 0 – 180° , we find three clear maxima for both surfaces at angles of about

30° , 90° , and 150° (we estimate an error of $\pm 2.5^\circ$ for the angle measurement), in agreement with the expectation from the 3-fold surface symmetry and the optimum adsorption geometry. Additionally, three minor peaks with maxima at about 0° , 60° , and 120° can be identified in the bulk data. These peaks are not clearly apparent from the thin film surface data, however; we explain this by the reduced total number of orientations extracted from the thin film experiments.

The minor peaks can be explained by the energetically second-best DFT-optimized geometry geo 2 (see the Supporting Information Figure S3 for models of all further calculated geometries); the top and side views of this geometry are shown in Figure 4c,d. Compared to geo 1, the calculated adsorption energy is reduced by 0.16 eV. For this geometry geo 2, the carboxylic acid moiety A is found in a position very similar to the one in geo 1, namely, in-plane with the close-by Cp ring binding to F_{top} and Ca surface atoms, while the other carboxylic acid moiety B is rotated by more than 180° around the $\text{C}_{\text{COOH}}\text{--C}_{\text{Cp}}$ bond. In particular, a bond between the carbonyl oxygen and the Ca surface atom is still present as in geo 1; however, the hydroxyl group moves toward the molecular center and binds to F_{top} underneath the molecular iron. As a consequence, the FDCA molecule adapts a partly staggered conformation with the Cp–Fe–Cp axis oriented at about 30° with respect to the $[11\bar{2}]$ direction. The staggered Cp rings also cause the protrusion of only one hydrogen atom per Cp ring into the vacuum; yet, due to the staggered ring orientation, the two protruding hydrogen atoms are at different ring positions. When drawing a line along these two hydrogen atoms, we find an angle of about 60° with respect to the $[11\bar{2}]$ directions, 30° off the hydrogen orientation found in geo 1, causing intermediate orientations. Thus, the flexibility of the FDCA molecule enables the experimental observation of at least two molecular geometries with their experimental occurrence frequency reflecting the order of the DFT-calculated adsorption energies. More importantly, however, we find a retention of the bond formation between the carboxylic acid moieties and the top-layer surface ions, which additionally highlights the strong templating effect of the substrate.

Finally, a comparably small molecule–molecule interaction is identified from a DFT-based analysis of molecular dimers and an experimental measurement of the nearest-neighbor distances. Three molecular dimer geometries were considered with DFT using the optimum adsorption geometry geo 1 as the starting point with results presented in Figure 5. Two FDCA molecules were arranged either along the $[\bar{1}10]$ (see Figure 5a) or along the $[11\bar{2}]$ (see Figure 5b) direction, as well as in a closely interlaced geometry (see Figure 5c). We note that arranging molecules along $[\bar{1}10]$ separated by $a = 770$ pm and along $[11\bar{2}]$ with a spacing of $b = 670$ pm leads to a $(2\sqrt{2} \times \sqrt{2})R45^\circ$ superstructure. From the calculations, we find that the molecules in the dimer geometries move slightly together by about 55 pm for the $[\bar{1}10]$ dimer orientation (see Figure 5a) and by about 25 pm for a dimer along $[11\bar{2}]$ (see Figure 5b), while they move apart by more than 170 pm from a starting distance of 386 pm for the interlaced dimer geometry (see Figure 5c). This geometrical rearrangement agrees with an analysis of the dimer binding energies, where we find an energy gain of about -0.08 and -0.14 eV for the $[\bar{1}10]$ and $[11\bar{2}]$ dimers, respectively, while the interlaced dimer is energetically unfavored with an energy loss of about 0.09 eV. For all

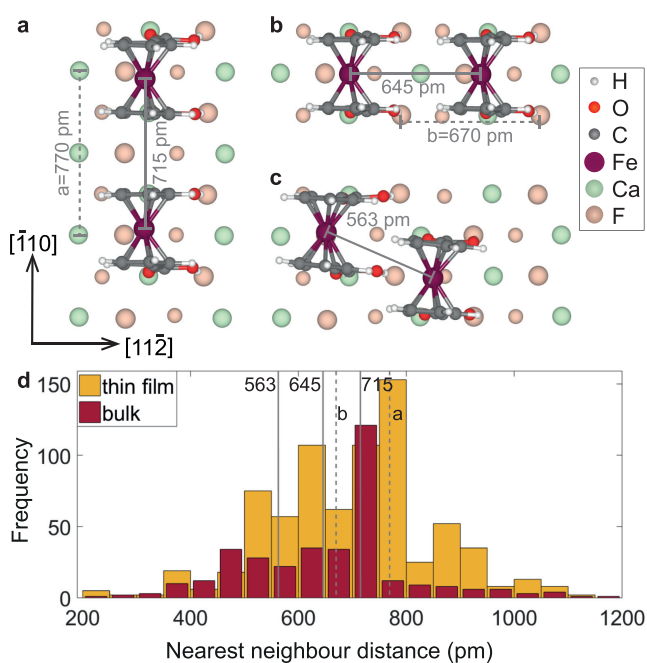


Figure 5. Analysis of molecular distances. (a–c) Top views of DFT-optimized geometries for FDCA dimer arrangements. (d) Nearest-neighbor distance distribution extracted from NC-AFM and STM images. Results for bulk (thin film) samples are plotted in red (yellow). DFT-calculated dimer distances are indicated in (a)–(d) by solid gray lines. Dashed gray lines are used in all panels to indicate the size of a $(2\sqrt{2} \times \sqrt{2})R45^\circ$ superstructure.

geometries, the quadruped molecule–surface anchoring motif remains with only minor geometrical rearrangements.

The dimer distances are very well reproduced by our experiments. A total of 352 (756) molecular pairs were measured on the bulk (thin film) surfaces, and we observe a clear accumulation of molecular separations at about 500–800 pm with a maximum of around 750 pm (we estimate an error of ± 50 pm in all measurements); see Figure 5d. Especially, the DFT-calculated dimer distances of 563 pm, 645 pm, and 715 pm, as well as the unit cell sizes $a = 770$ pm and $b = 670$ pm of a $(2\sqrt{2} \times \sqrt{2})R45^\circ$ superstructure, lie within the experimental nearest-neighbor distance distribution.

Comparing the energy gain of up to -0.14 eV due to dimer formation with the adsorption energy of -1.74 eV due to the quadruped anchoring directly highlights a significantly stronger molecule–surface than molecule–molecule interaction in agreement with the experimental observations.

CONCLUSIONS

FDCA molecules on $\text{CaF}_2(111)$ bind to the top fluorine and top calcium surface atoms via their carboxylic acid moieties, forming F–HO hydrogen, as well as Ca–O bonds in a quadruped geometry. The bond formation is facilitated by an excellent match of the molecular moiety dimensions with the surface lattice sizes and leads to an upright, slightly tilted molecular geometry with firm anchoring to the surface. The majority of FDCA molecules is found to adapt this geometry, with three different molecular orientations following the 3-fold rotational symmetry of the $\text{CaF}_2(111)$ surface. However, an energetically second-best molecular geometry, where one molecular carboxylic acid moiety is rotated by about 180° , is present as a minority population. The quadruped molecular

adsorption geometry at equivalent lattice sites on the surface is maintained when considering molecular dimers in DFT; weak molecule–molecule interactions cause only slight molecular relaxations. The calculated dimer distances are in agreement with the experimentally observed nearest-neighbor distance distribution. No nucleation at surface defect sites on $\text{CaF}_2(111)$ terraces was found, and no differences between adsorption on bulk and thin film surfaces were apparent in the experimental data. The latter observation is in full agreement with DFT calculations, where surface ion displacements and electron density differences revealed a confinement of the molecule–substrate interaction to mostly the first CaF_2 substrate layer.

In conclusion, we identified a strong templating effect facilitated by a quadruped anchoring motif for the FDCA/ $\text{CaF}_2(111)$ system. The robustness of the anchoring mechanism is evidenced by the observation of small molecular clusters and single molecules stable at room temperature, observed on both bulk $\text{CaF}_2(111)$ and thin film $\text{CaF}_2/\text{CaF}_1/\text{Si}(111)$ surfaces. The room-temperature stability together with the possibility for structure formation on device-relevant CaF_2 thin films⁴⁴ makes this system highly relevant for applications. Thus, our findings open the door to advanced molecular adsorption and reaction studies, exploiting the anchoring motif found here on $\text{CaF}_2(111)$. The vertical arrangement of carboxylic acid groups to form a strong molecule–surface bond could further be exploited to anchor larger functional structures or to grow self-assembled monolayers on an optically transparent insulator surface.

ASSOCIATED CONTENT

Supporting Information

The Supporting Information is available free of charge at <https://pubs.acs.org/doi/10.1021/acs.jpcc.0c00115>.

Geometry optimization; FDCA gas-phase geometries; adsorption geometries geo 4 to geo 8 of FDCA on $\text{CaF}_2(111)$; and DFT-calculated adsorption energy E_{ads} and adsorption angles α and α' of FDCA on $\text{CaF}_2(111)$ (PDF).

AUTHOR INFORMATION

Corresponding Author

Philipp Rahe – *Fachbereich Physik, Universität Osnabrück, 49076 Osnabrück, Germany*; orcid.org/0000-0002-2768-8381; Phone: +49 (0)541 969-2261; Email: prahe@uni-osnabrueck.de

Authors

Linda Laflör – *Fachbereich Physik, Universität Osnabrück, 49076 Osnabrück, Germany*
 Fabian A. Schlage – *Fachbereich Physik, Universität Osnabrück, 49076 Osnabrück, Germany*
 Lev Kantorovich – *Department of Physics, King's College London, London WC2R 2LS, United Kingdom*; orcid.org/0000-0001-9379-6834
 Philip J. Moriarty – *School of Physics and Astronomy, The University of Nottingham, Nottingham NG7 2RD, United Kingdom*
 Michael Reichling – *Fachbereich Physik, Universität Osnabrück, 49076 Osnabrück, Germany*

Complete contact information is available at:

<https://pubs.acs.org/doi/10.1021/acs.jpcc.0c00115>

Notes

The authors declare no competing financial interest.

ACKNOWLEDGMENTS

Financial support by the German Research Foundation (DFG) via grant RA2832/1-1 and from the People Programme (Marie Curie Actions) of the European Union's Seventh Framework Programme (FP7/2007-2013) under Research Executive Agency (REA) Grant No. 628439 is gratefully acknowledged. P.R. thanks Samuel Jarvis (Lancaster University, U.K.) and Matthew Watkins (University of Lincoln, U.K.) for the most helpful advice on CP2K, the CP2K-UK project for strong support, and David Abbasi-Pérez (King's College London, U.K.) for the most helpful assistance on calculating and presenting electron density differences. Computing time was granted by the University of Osnabrück via DFG project 239246210.

REFERENCES

- (1) Barth, J. V. Molecular architectonic on metal surfaces. *Annu. Rev. Phys. Chem.* **2007**, *58*, 375–407.
- (2) Kühnle, A. Self-assembly of organic molecules at metal surfaces. *Curr. Opin. Colloid Interface Sci.* **2009**, *14*, 157–168.
- (3) Maurer, R. J.; Ruiz, V. G.; Camarillo-Cisneros, J.; Liu, W.; Ferri, N.; Reuter, K.; Tkatchenko, A. Adsorption structures and energetics of molecules on metal surfaces: Bridging experiment and theory. *Prog. Surf. Sci.* **2016**, *91*, 72–100.
- (4) Barth, C.; Foster, A. S.; Henry, C. R.; Shluger, A. L. Recent trends in surface characterization and chemistry with high-resolution scanning force methods. *Adv. Mater.* **2011**, *23*, 477–501.
- (5) Bombis, C.; Ample, F.; Lafferentz, L.; Yu, H.; Hecht, S.; Joachim, C.; Grill, L. Single molecular wires connecting metallic and insulating surface areas. *Angew. Chem., Int. Ed.* **2009**, *48*, 9966–9970.
- (6) Rahe, P.; Steele, R. P.; Williams, C. C. Consecutive charging of a molecule-on-insulator ensemble using single electron tunnelling methods. *Nano Lett.* **2016**, *16*, 911–916.
- (7) Steurer, W.; Fatayer, S.; Gross, L.; Meyer, G. Probe-based measurement of lateral single-electron transfer between individual molecules. *Nat. Commun.* **2015**, *6*, No. 8353.
- (8) Burke, S. A.; Topple, J. M.; Grütter, P. Molecular dewetting on insulators. *J. Phys.: Condens. Matter* **2009**, *21*, No. 423101.
- (9) Rahe, P.; Kittelmann, M.; Neff, J. L.; Nimmrich, M.; Reichling, M.; Maass, P.; Kühnle, A. Tuning molecular self-assembly on bulk insulator surfaces by anchoring of the organic building blocks. *Adv. Mater.* **2013**, *25*, 3948–3956.
- (10) Para, F.; Bocquet, F.; Nony, L.; Loppacher, C.; Féron, M.; Cherioux, F.; Gao, D. Z.; Federici Canova, F.; Watkins, M. B. Micrometre-long covalent organic fibres by photoinitiated chain-growth radical polymerization on an alkali-halide surface. *Nat. Chem.* **2018**, *10*, 1112–1117.
- (11) Lindner, R.; Kühnle, A. On-surface reactions. *ChemPhysChem* **2015**, *16*, 1582–1592.
- (12) Rahe, P.; Nimmrich, M.; Kühnle, A. Substrate templating upon self-assembly of hydrogen-bonded molecular networks on an insulating surface. *Small* **2012**, *8*, 2968.
- (13) Maier, S.; Fendt, L.-A.; Zimmerli, L.; Glatzel, T.; Pfeiffer, O.; Diederich, F.; Meyer, E. Nanoscale engineering of molecular porphyrin wires on insulating surfaces. *Small* **2008**, *4*, 1115–1118.
- (14) Amrous, A.; Bocquet, F.; Nony, L.; Para, F.; Loppacher, C.; Lamare, S.; Palmino, F.; Cherioux, F.; Gao, D. Z.; Canova, F. F. Molecular design and control over the morphology of self-assembled films on ionic substrates. *Adv. Mater. Interfaces* **2014**, *1*, No. 1400414.
- (15) Paris, C.; Floris, A.; Aeschlimann, S.; Kittelmann, M.; Kling, F.; Bechstein, R.; Kühnle, A.; Kantorovich, L. Increasing the templating effect on a bulk insulator surface: from a kinetically trapped to a thermodynamically more stable structure. *J. Phys. Chem. C* **2016**, *120*, 17546–17554.
- (16) Schütte, J.; Bechstein, R.; Rohlfing, M.; Reichling, M.; Kühnle, A. Cooperative mechanism for anchoring highly polar molecules at an ionic surface. *Phys. Rev. B* **2009**, *80*, No. 205421.
- (17) Loske, F.; Reichling, M.; Kühnle, A. Deposition sequence determines morphology of C₆₀ and 3,4,9,10-Perylenetetracarboxylic diimide islands on CaF₂(111). *Jpn. J. Appl. Phys.* **2011**, *50*, No. 08LB07.
- (18) Loske, F.; Reichling, M.; Kühnle, A. Steering molecular island morphology on an insulator surface by exploiting sequential deposition. *Chem. Commun.* **2011**, *47*, 10386–10388.
- (19) Gritzner, G.; Kuta, J. Recommendations on reporting electrode potentials in nonaqueous solvents (Recommendations 1983). *Pure Appl. Chem.* **1984**, *56*, 461.
- (20) Berger, J.; Košmider, K.; Stetsovych, O.; Vondráček, M.; Hapala, P.; Spadafora, E. J.; Švec, M.; Jelínek, P. Study of ferrocene dicarboxylic acid on substrates of varying chemical activity. *J. Phys. Chem. C* **2016**, *120*, 21955–21961.
- (21) Rahe, P.; Smith, E. F.; Wollschläger, J.; Moriarty, P. J. Formation routes and structural details of the CaF₁ layer on Si(111) from high-resolution noncontact atomic force microscopy data. *Phys. Rev. B* **2018**, *97*, No. 125418.
- (22) Tröger, L.; Schütte, J.; Ostendorf, F.; Kühnle, A.; Reichling, M. Concept for support and cleavage of brittle crystals. *Rev. Sci. Instrum.* **2009**, *80*, No. 063703.
- (23) Giessibl, F. J. High-speed force sensor for force microscopy and profilometry utilizing a quartz tuning fork. *Appl. Phys. Lett.* **1998**, *73*, 3956–3958.
- (24) Majzik, Z.; Setvín, M.; Bettac, A.; Feltz, A.; Cháb, V.; Jelínek, P. Simultaneous current, force and dissipation measurements on the Si(111) 7x7 surface with an optimized qPlus AFM/STM technique. *Beilstein J. Nanotechnol.* **2012**, *3*, 249–259.
- (25) Nečas, D.; Klapetek, P. Gwyddion: an open-source software for SPM data analysis. *Open Phys.* **2012**, *10*, 181–188.
- (26) Hutter, J.; Iannuzzi, M.; Schiffrmann, F.; VandeVondele, J. CP2K: atomistic simulations of condensed matter systems. *Wiley Interdiscip. Rev.: Comput. Mol. Sci.* **2014**, *4*, 15–25.
- (27) VandeVondele, J.; Hutter, J. Gaussian basis sets for accurate calculations on molecular systems in gas and condensed phases. *J. Chem. Phys.* **2007**, *127*, No. 114105.
- (28) Lippert, G.; Hutter, J.; Parrinello, M. The Gaussian and augmented-plane-wave density functional method for ab initio molecular dynamics simulations. *Theor. Chem. Acc.* **1999**, *103*, 124–140.
- (29) Krack, M. Pseudopotentials for H to Kr optimized for gradient-corrected exchange-correlation functionals. *Theor. Chem. Acc.* **2005**, *114*, 145–152.
- (30) Perdew, J. P.; Burke, K.; Ernzerhof, M. Generalized gradient approximation made simple. *Phys. Rev. Lett.* **1996**, *77*, 3865–3868.
- (31) Grimme, S.; Antony, J.; Ehrlich, S.; Krieg, H. A consistent and accurate ab initio parametrization of density functional dispersion correction (DFT-D) for the 94 elements H-Pu. *J. Chem. Phys.* **2010**, *132*, No. 154104.
- (32) Sabatini, R.; Gorni, T.; de Gironcoli, S. Nonlocal van der Waals density functional made simple and efficient. *Phys. Rev. B* **2013**, *87*, No. 041108.
- (33) Boys, S. F.; Bernardi, F. The calculation of small molecular interactions by the differences of separate total energies. Some procedures with reduced errors. *Mol. Phys.* **1970**, *19*, 553–566.
- (34) Barth, C.; Foster, A. S.; Reichling, M.; Shluger, A. L. Contrast formation in atomic resolution scanning force microscopy on CaF₂(111): experiment and theory. *J. Phys.: Condens. Matter* **2001**, *13*, 2061–2079.
- (35) Foster, A. S.; Barth, C.; Shluger, A. L.; Reichling, M. Unambiguous interpretation of atomically resolved force microscopy images of an insulator. *Phys. Rev. Lett.* **2001**, *86*, 2373–2376.
- (36) Wollschläger, J. *Recent Research Developments in Applied Physics*; Pandalai, S., Ed.; Transworld Research Network: Trivandrum, India, 2002; Vol. 5-II, pp 621–695.

(37) Olmstead, M. A. *Thin Films: Heteroepitaxial Systems*; Liu, W. K.; Santos, M. B., Eds.; World Scientific: Singapore, 1999; Chapter 5; Vol. 15.

(38) Loppacher, C.; Zerweck, U.; Eng, L. M.; Gemming, S.; Seifert, G.; Olbrich, C.; Morawetz, K.; Schreiber, M. Adsorption of PTCDA on a partially KBr covered Ag(111) substrate. *Nanotechnology* **2006**, *17*, 1568–1573.

(39) Kunstmann, T.; Schlarb, A.; Fendrich, M.; Wagner, T.; Möller, R.; Hoffmann, R. Dynamic force microscopy study of 3,4,9,10-perylenetetracarboxylic dianhydride on KBr(001). *Phys. Rev. B* **2005**, *71*, No. 121403.

(40) Such, B.; Goryl, G.; Godlewski, S.; Kolodziej, J. J.; Szymonski, M. PTCDA molecules on a KBr/InSb system: a low temperature STM study. *Nanotechnology* **2008**, *19*, No. 475705.

(41) Palenik, G. J. Crystal and molecular structure of ferrocenedicarboxylic acid. *Inorg. Chem.* **1969**, *8*, 2744–2749.

(42) Takusagawa, F.; Koetzle, T. F. Crystal and molecular-structure of 1,1'-Ferrocenedicarboxylic acid (triclinic modification) - Neutron and X-ray-diffraction studies at 78K and 298K. *Acta Crystal. Sec. B* **1979**, *35*, 2888–2896.

(43) Steiner, T. The hydrogen bond in the solid state. *Angew. Chem., Int. Ed.* **2002**, *41*, 48–76.

(44) Illarionov, Y. Y.; Banskchikov, A. G.; Polyushkin, D. K.; Wachter, S.; Knobloch, T.; Thesberg, M.; Mennel, L.; Paur, M.; Stöger-Pollach, M.; Steiger-Thirsfeld, A.; et al. Ultrathin calcium fluoride insulators for two-dimensional field-effect transistors. *Nat. Electron.* **2019**, *2*, 230–235.